AIMS Mathematics, 10(12): 30134–30161.
DOI: 10.3934/math.20251324
Received: 28 September 2025
Revised: 08 December 2025
Accepted: 19 December 2025
Published: 24 December 2025

https://www.aimspress.com/journal/Math

Research article

A novel spectral framework for stochastic differential equations: leveraging shifted Vieta-Fibonacci polynomials

Ahmed G. Khattab[1], D.A. Hammad[1], Mourad S. Semary[1,2], Emad A. Mohamed[3,*], Iram Malik[3] and Aisha F. Fareed[3]

[1] Basic Engineering Sciences Department, Benha Faculty of Engineering, Benha University, Benha 13512, Egypt
[2] Basic Sciences Department, Faculty of Engineering, Badr University in Cairo BUC, Cairo 11829, Egypt
[3] Department of Electrical Engineering, College of Engineering, Prince Sattam bin Abdulaziz University, Al Kharj 11942, Saudi Arabia

* **Correspondence:** Email: e.younis@psau.edu.sa.

Abstract: In this paper, we introduced a novel numerical approach for solving stochastic heat equations and multi-dimensional stochastic Poisson equations using shifted Vieta-Fibonacci polynomials (SVFPs), marking their first application in stochastic differential equations. The proposed method leveraged the orthogonality and recurrence properties of SVFPs to approximate solutions with high precision. By normalizing the polynomial basis and their derivatives, the technique ensured numerical stability and convergence, addressing challenges encountered in earlier implementations. The method was rigorously validated through comparisons with the fast discrete Fourier transform approach, other methods in the literature, and, where applicable, exact solutions, demonstrating superior accuracy. Five illustrative problems were analyzed, with results showcasing significantly reduced variance and absolute errors, particularly for higher-order approximations. The numerical simulations, executed using *Mathematica 12*, highlighted the robustness of the SVFPs-based algorithm in handling stochastic variability. This work not only extended the applicability of SVFPs to stochastic domains but also provided a reliable framework for future research on fractional and nonlinear stochastic systems.

Keywords: Vieta-Fibonacci polynomials; orthogonal polynomials; heat equation; Poisson equation; stochastic differential equations; white noise
Mathematics Subject Classification: 65C30, 65L12

Abbreviations:

PDEs: partial differential equations; SPDEs: stochastic partial differential equations; SHE: stochastic heat equation; SPE: stochastic Poisson equation; BCs: boundary conditions; 2D: two dimensions; 3D: three dimensions; VFPs: Vieta-Fibonacci polynomials: SVFPs: shifted Vieta-Fibonacci polynomials; FDFT: fast discrete Fourier transform; TNPCS: ten non-polynomial cubic spline; QIMD: quasi-inverse matrix diagonalization

1. Introduction

The mathematical modeling of physical phenomena is fundamental to advancement in science and engineering, providing a framework to predict, optimize, and understand complex systems. Central to this endeavor are partial differential equations (PDEs), among which the heat equation and the Poisson equation stand as two of the most profound and universally applicable. The heat equation, a cornerstone of mathematical physics, is a parabolic PDE that describes the distribution of heat (or any diffusing quantity) in a region over time. Its deterministic form has been extensively studied due to its broad applicability in fields such as thermodynamics, material science, and biological systems, where it describes phenomena such as thermal conduction, diffusion processes, and chemical gradients [1]. Beyond these traditional domains, it has a pivotal role in cutting-edge fields, including quantum field theory, turbulence, signal processing, and population dynamics [1,2].

The Poisson equation is a fundamental elliptic PDE that models how a field (e.g., potential, temperature, and pressure) is influenced by distributed sources throughout a domain. It is widely applicable in numerous disciplines [3–6], including electrostatics (computing the electrostatic potential from charge distributions), magnetism (describing magnetic potential fields), mechanical engineering (modeling stress, strain, and heat conduction problems), fluid dynamics (linking pressure and velocity fields and describing potential flows), heat conduction (determining temperature distributions in steady-state scenarios), astrophysics and gravity (describing gravitational potential from mass distributions), and additive manufacturing (modeling heat conduction with moving sources, such as laser heads).

The stochastic partial differential equations (SPDEs) are the mathematical framework that combines the deterministic structure of PDEs with the randomness inherent in stochastic differential equations. Generally, SPDEs involve randomness in one or more components, such as their coefficients, initial or boundary conditions, driving forces such as a noise term, or the domain in which they are defined. In our study, we emphasize SPDEs with a driving force associated with white noise that influences the behavior of the solution.

However, real-world phenomena often involve inherent uncertainties due to external fluctuations, measurement errors, or environmental noise. To account for these stochastic influences, the deterministic heat and Poisson equations were extended to incorporate random terms, leading to the stochastic heat equation (SHE) and the stochastic Poisson equation (SPE). Solving SPDEs presents significant challenges due to the interplay between diffusion and noise. Unlike deterministic PDEs, stochastic counterparts rarely admit closed-form solutions, necessitating the development of robust numerical and analytical techniques. Advances in computational mathematics have introduced various

methods to approximate solutions to such equations. Among these, the fast discrete Fourier transform (FDFT) method [7] and the ten non-polynomial cubic spline (TNPCS) approach [8,9] have demonstrated efficacy in handling stochastic terms. Other notable techniques include operational matrices based on Legendre polynomials [10], spectral stochastic methods [11], the stochastic exponential method [12], the finite element and Tau-finite difference approach[13,14], and the Galerkin collocation hybrid method [15]. Additionally, specialized approaches such as the stochastic improved Simpson [16], conformable fractional discrete Temimi–Ansari techniques [17], and integral transform-based homotopy perturbation methods [18] have further enriched the toolkit for solving stochastic differential systems. Additionally, the finite difference and the meshfree methods are used to approximate the 2D stochastic time-fractional Sine–Gordon equation on the non-rectangular domains [19].

In this work, we introduce a novel numerical approach based on shifted Vieta-Fibonacci polynomials (SVFPs) to approximate solutions to the SHE and multi-dimensional SPE. Vieta-Fibonacci polynomials (VFPs), named in honor of the mathematicians François Viète and Leonardo Fibonacci, are a class of orthogonal polynomials with deep connections to Fibonacci sequences and Chebyshev polynomials. VFPs have gained attention for their effectiveness in solving fractional-order differential and integro-differential equations, including the fractional Korteweg-de Vries (KdV) equation, advection-reaction-diffusion problems, and pantograph equations [20–26]. However, their application to stochastic differential equations, particularly those involving white noise, remains unexplored. This study bridges that gap by presenting the first systematic application of SVFPs to stochastic heat equations, offering a new perspective on noise-driven PDEs. In this work, we present a novel application of VFPs in the stochastic domain related to white noise analysis. This marks the first exploration of VFPs in such a setting, presenting a notable challenge. Ultimately, we successfully apply VFPs to the SHE, which takes the following forms as in [7,8]:

$$\frac{\partial}{\partial t}\psi(t,x) = \sigma\frac{\partial^2}{\partial x^2}\psi(t,x) + \varepsilon\frac{\partial}{\partial x}\psi(t,x) + \rho\psi(t,x)n(t), \tag{1.1}$$

$$\frac{\partial}{\partial t}\psi(t,x) = (\sigma + \rho n(t))\frac{\partial^2}{\partial x^2}\psi(t,x), \tag{1.2}$$

$$\psi(0,x) = g(x),\ \psi(t,0) = \psi(t,a) = 0,\ (t,x) \in [0,T] \times [a,b],$$

where σ, ε, and ρ are real constants, and $\psi(t,x)$ is the unknown function. The system includes a Gaussian-white-noise term $n(t) = \mu\frac{d}{dt}\mathcal{B}(t)$, with zero expectation and variance μ^2, and $\mathcal{B}(t)$ denotes the Brownian motion process, defined by the following characteristics: (i) It is a Gaussian process, (ii) it exhibits independent increments, and (iii) $t \to \mathcal{B}(t)$ is continuous with probability one.

Moreover, we applied VFPs to the muti-dimensional SPE defined as:

$$\boldsymbol{\nabla}_d\psi(\boldsymbol{x}) + \rho\, n(t) = f(\boldsymbol{x}),\ \boldsymbol{x} \in [a,b]^d, \tag{1.3}$$

with zero boundary conditions: $\psi = 0$, and the exact solution for $\rho = 0$ is: $\psi(\boldsymbol{x}) = \prod_{l=1}^{d}\sin(2\pi\boldsymbol{x_l})$, where $\boldsymbol{\nabla}_d$ is the Laplacian operator, $\psi(\boldsymbol{x})$ is the unknown function, and $n(t)$ is the Gaussian-white-noise. The parameter d stands for number of dimensions such that: $d = 2$ for 2D SPE, and the vector $\boldsymbol{x} = (x_1, x_2) \equiv (t,x)$ and $d = 3$ for 3D Poisson equation, and the vector $\boldsymbol{x} = (x_1, x_2, x_3) \equiv (t,x,y)$.

The major contributions of this work are as follows:

- **Derivation of a simplified first-order derivative operator** for SVFPs, facilitating efficient numerical implementation.
- **Normalization of SVFP bases** to enhance stability and convergence in stochastic settings.
- **Development of a novel SVFP-based algorithm** for solving SHE and SPE, incorporating white noise representation via SVFPs instead of traditional finite difference schemes [7,8].
- **Validation through comparative analysis**, demonstrating superior accuracy and computational efficiency over existing methods such as FDFT [7] and TNPCS [8].

The remainder of this paper is organized as follows: In Section 2, we introduce the mathematical foundations of SVFPs, including their recurrence relations, orthogonality properties, and derivative operators. In Section 3, we detail the numerical implementation of SVFPs for SHE and SPE, addressing challenges such as noise discretization and system normalization. In Section 4, we present numerical experiments, comparing the proposed method with benchmark techniques and analyzing error convergence. Finally, in Section 5, we conclude with a discussion of the method's broader implications and potential extensions to higher-dimensional and nonlinear stochastic systems.

This research not only advances the theoretical understanding of orthogonal polynomial methods in stochastic settings but also provides a computationally efficient framework for practical applications.

2. Theoretical foundations: shifted Vieta-Fibonacci polynomials in stochastic domains

Here, we define the VFPs and their shifted counterparts (SVFPs), highlighting their orthogonality properties and recurrence relations. We derive their connection to Chebyshev polynomials and establish the groundwork for their application in stochastic settings. Key focus areas include the explicit forms of SVFPs, weight functions, and their adaptation to bounded domains.

The VFPs denoted by $\mathcal{F}_\ell(x)$ are one of the orthogonal functions that may be defined as [20–27]:

$$\mathcal{F}_\ell(x) = \frac{\sin(\ell\varphi)}{\sin(\varphi)}, \tag{2.1}$$

where $\varphi = \cos^{-1}\left(\frac{x}{2}\right)$, $\varphi \in [0,\pi]$, $x \in [-2,2]$, and $\ell = 0,1,2,\ldots,M_x$. Their recurrence relation is:

$$\mathcal{F}_\ell(x) = x\mathcal{F}_{\ell-1}(x) - \mathcal{F}_{\ell-2}(x),\ \ell \geq 2, \tag{2.2}$$

where $\mathcal{F}_0(x) = 0$, and $\mathcal{F}_1(x) = 1$. Moreover, VFPs can be defined as a function of Chebyshev polynomials of the second kind $\left(U_\ell(x)\right)$ as:

$$\mathcal{F}_\ell(x) = U_{\ell-1}\left(\frac{x}{2}\right),\ \ell \geq 1, \tag{2.3}$$

where $U_0(x) = 1$, $U_1(x) = 2x$, and for $n \geq 2$, $U_n(x) = 2x\,U_{n-1}(x) - U_{n-2}(x)$.

VFPs explicit formula is:

$$\mathcal{F}_\ell(x) = \sum_{k=0}^{\left\lfloor\frac{\ell-1}{2}\right\rfloor}(-1)^k\left(\frac{(\ell-k-1)!}{k!\,(\ell-2k-1)!}\right)x^{\ell-2k-1},\ \ell \geq 1, \tag{2.4}$$

where $\left\lfloor\frac{\ell-1}{2}\right\rfloor$ represents the floor function.

VFPs are orthogonal over interval $[-2, 2]$ and their orthogonality condition is:

$$\langle \mathcal{F}_\ell(x), \mathcal{F}_m(x) \rangle_\omega = \int_{-2}^{2} \mathcal{F}_\ell(x)\mathcal{F}_m(x)\omega(x)dx = (2\pi)\delta_{\ell m} = \begin{cases} 2\pi, & \ell = m, \\ 0, & \ell \neq m, \end{cases} \tag{2.5}$$

where $\omega(x) = \sqrt{4 - x^2}$ represents the weight function of VFPs.

SVFPs denoted by $\tilde{\mathcal{F}}_\ell(x)$ represent VFPs over $x \in [a, b]$ using a linear transformation: $\tilde{x} = \left(\frac{2}{b-a}\right)[2x - (a + b)]$. The recurrence relation of SVFPs is defined as:

$$\tilde{\mathcal{F}}_0(x) = 0, \ \tilde{\mathcal{F}}_1(x) = 1,$$
$$\tilde{\mathcal{F}}_\ell(x) = \left(\frac{2}{b-a}\right)[2x - (a + b)]\tilde{\mathcal{F}}_{\ell-1}(x) - \tilde{\mathcal{F}}_{\ell-2}(x), \ \ell \geq 2. \tag{2.6}$$

Additionally, SVFPs are orthogonal with the weight function $\tilde{\omega}(x) = \sqrt{(b - x)(x - a)}$, defined as:

$$\langle \tilde{\mathcal{F}}_\ell(x), \tilde{\mathcal{F}}_m(x) \rangle_\omega = \int_0^a \tilde{\mathcal{F}}_\ell(x)\tilde{\mathcal{F}}_m(x)\tilde{\omega}(x)dx = \frac{\pi}{8}(b - a)^2\delta_{\ell m} = \begin{cases} \left(\frac{\pi}{8}\right)(b - a)^2, & \ell = m, \\ 0, & \ell \neq m. \end{cases} \tag{2.7}$$

This part presents a streamlined derivation of first- and higher-order derivative operators for SVFPs, expressed in matrix form for computational efficiency. We demonstrate how these operators enable efficient discretization of spatial derivatives, contrasting them with traditional finite-difference approximations. The first-order derivative of SVFPs is derived and implemented in a novel, simplified form to facilitate efficient application to enabling efficient application to the SHE, SPE, and other related problems. Its implicit formula is defined as:

$$D^{(1)}\left(\tilde{\mathcal{F}}_\ell(x)\right) = \left(\frac{4}{b-a}\right)\sum_{k=1}^{\left\lfloor \frac{\ell}{2} \right\rfloor}(\ell - 2k + 1)\tilde{\mathcal{F}}_{\ell-2k+1}(x), \ \ell = 1, 2, 3, \ldots, M_x, \tag{2.8}$$

alternatively, in matrix form, it is expressed as:

$$D^{(1)}\left(\tilde{\mathcal{F}}_i(x)\right) = \left(\frac{4}{b-a}\right)D^{(1)}_{m,i}\tilde{\mathcal{F}}, \tag{2.9}$$

where $m = 0, 1, 2, \ldots, M_x - 1, \ i = 1, 2, 3, \ldots, M_x,$

$$\tilde{\mathcal{F}} = [\tilde{\mathcal{F}}_1(x), \tilde{\mathcal{F}}_2(x), \tilde{\mathcal{F}}_3(x), \ldots, \tilde{\mathcal{F}}_{Mx-1}(x), \tilde{\mathcal{F}}_{Mx}(x)]^T,$$

and $D^{(1)}_{m,i} = \begin{cases} 0, & m = 0, \\ i, & m \neq 0 \wedge i \leq m \wedge (m - i) \text{ is even}, \\ 0, & \text{otherwise}. \end{cases}$

The second-order derivative of SVFPs is derived by applying the first-order derivative operator twice and is expressed as:

$$D^{(2)}\left(\tilde{\mathcal{F}}_\ell(x)\right) = D^{(1)} \times D^{(1)}\left(\tilde{\mathcal{F}}_\ell(x)\right) = \left(\frac{4}{b-a}\right)^2\left(D^{(1)}_{m,i} \times D^{(1)}_{m,i}\right)\tilde{\mathcal{F}}. \tag{2.10}$$

In general, the k^{th}-order derivative of SVFPs is given as:

$$D^{(k)}\left(\tilde{\mathcal{F}}_{\ell}(x)\right)=\underbrace{D^{(1)}\times D^{(1)}\times\ldots\times D^{(1)}}_{k\text{ times}}\left(\tilde{\mathcal{F}}_{\ell}(x)\right)=\left(\frac{4}{b-a}\right)^{k}\left(\underbrace{D_{m,i}^{(1)}\times D_{m,i}^{(1)}\times\ldots\times D_{m,i}^{(1)}}_{k\text{ times}}\right)\tilde{\mathcal{F}}. \quad (2.11)$$

For $M_x=10$, the first-order and second-order derivative operators of SVFPs are numerically expressed as:

$$D^{(1)}=\left(\frac{4}{b-a}\right)\begin{bmatrix}0&0&0&0&0&0&0&0&0&0\\1&0&0&0&0&0&0&0&0&0\\0&2&0&0&0&0&0&0&0&0\\1&0&3&0&0&0&0&0&0&0\\0&2&0&4&0&0&0&0&0&0\\1&0&3&0&5&0&0&0&0&0\\0&2&0&4&0&6&0&0&0&0\\1&0&3&0&5&0&7&0&0&0\\0&2&0&4&0&6&0&8&0&0\\1&0&3&0&5&0&7&0&9&0\end{bmatrix},$$

and

$$D^{(2)}=\left(\frac{4}{b-a}\right)^{2}\begin{bmatrix}0&0&0&0&0&0&0&0&0&0\\0&0&0&0&0&0&0&0&0&0\\2&0&0&0&0&0&0&0&0&0\\0&6&0&0&0&0&0&0&0&0\\6&0&12&0&0&0&0&0&0&0\\0&16&0&20&0&0&0&0&0&0\\12&0&30&0&30&0&0&0&0&0\\0&30&0&48&0&42&0&0&0&0\\20&0&54&0&70&0&56&0&0&0\\0&48&0&84&0&96&0&72&0&0\end{bmatrix}.$$

The proof of L_2 convergence of the SVFPS as in [27] can be summarized as following:

For $x\in[0,1]$, assume a given function, $\psi(x)\in L_{\widetilde{\omega}}^{2}[0,1]$, is defined as:

$$\psi(x)=\sum_{m=1}^{M+1}\tilde{\mathcal{F}}_m(x)\upsilon_m=\tilde{\mathcal{F}}(x)\mathcal{V},$$

where J is the number of subintervals in the given domain, $\widetilde{\omega}$ denotes the weight of SVFPs, L^2 represents L_2 -norm, $\tilde{\mathcal{F}}(x)=\left[\tilde{\mathcal{F}}_1(x),\tilde{\mathcal{F}}_2(x),\tilde{\mathcal{F}}_3(x),\ldots,\tilde{\mathcal{F}}_J(x),\tilde{\mathcal{F}}_{J+1}(x)\right]^T$, and $\mathcal{V}$ is a vector of unknowns given as: $\mathcal{V}=\left[\upsilon_1,\upsilon_2,\upsilon_3,\ldots,\upsilon_J,\upsilon_{J+1}\right]^T$.

Moreover, consider $\mathbb{V}_J=\mathrm{Span}\left\langle\tilde{\mathcal{F}}_1(x),\tilde{\mathcal{F}}_2(x),\tilde{\mathcal{F}}_3(x),\ldots,\tilde{\mathcal{F}}_{J+1}(x)\right\rangle$ and denote the space spanned by the SVFPs bases.

Theorem 1. [27] *Let assume that* $\psi\in C^J[0,1]$ *and* $P_J(x)$ *denotes the interpolating function of* ψ *at* J *Chebyshev points in interval* $[0,1]$*, Then, for every* $x\in[0,1]$*, we have*

$$\left|\psi(x)-P_J(x)\right|\leq\frac{M_{\psi,J}}{2^{(2J+1)}(J!)},\ M_{\psi,J}=\max_{\xi\in[0,1]}\left|\psi^{(J)}(\xi)\right|.$$

Theorem 2. [27] *Suppose that* $\psi\in C^{J+1}[0,1]\cap L_{\widetilde{\omega}}^{2}[0,1]$. *If* $\psi_J(x)=\widetilde{\mathcal{F}_J}(x)\mathcal{V}$ *denotes the best approximation of* $\psi(x)$ *out of* $\mathbb{V}_J$*, we have*

$$\lim_{J\to\infty}\|\psi-\psi_J\|_{\widetilde{\omega}}=0.$$

Proof of Theorem 2.

$$\|\psi(x)-\psi_J(x)\|_{\widetilde{\omega}}^2\le\|\psi(x)-P_J(x)\|_{\widetilde{\omega}}^2=\int_0^1|\psi(x)-P_J(x)|^2\widetilde{\omega}(x)dx$$

$$=\int_0^1\left(\frac{M_{\psi,J}}{2^{(2J+1)}(J!)}\right)^2\widetilde{\omega}(x)dx=\left(\frac{M_{\psi,J}}{2^{(2J+1)}(J!)}\right)^2\int_0^1\widetilde{\omega}(x)dx=\left(\frac{M_{\psi,J}}{2^{(2J+1)}(J!)}\right)^2\left(\frac{\pi}{8}\right).$$

Hence,

$$\|\psi(x)-\psi_J(x)\|_{\widetilde{\omega}}\le\left(\frac{M_{\psi,J}}{2^{(2J+1)}(J!)}\right)\sqrt{\frac{\pi}{8}},\ \lim_{J\to\infty}\|\psi-\psi_J\|_{\widetilde{\omega}}\to 0.$$

3. Methodology: a spectral approach to stochastic heat and muti-dimensional stochastic Poisson equations

3.1. Discretizing functions and noise with SVFPs

We propose a novel technique to represent functions and white noise using SVFP expansions, eliminating the need for finite-difference-based noise discretization. The Brownian motion process is approximated via SVFP series, and its derivative (white noise) is analytically computed using the derived SVFP differentiation matrices.

The SVFPs can be utilized to approximate the functions $\psi(t,x)$ and $\psi(t,x,y)$ as follows:

$$\psi(t,x)=\sum_{n=1}^{M_t+1}\sum_{m=1}^{M_x+1}\tilde{\mathcal{F}}_n(t)\tilde{\mathcal{F}}_m(x)\upsilon_{nm},\tag{3.1}$$

$$\psi(t,x,y)=\sum_{n=1}^{M_t+1}\sum_{m=1}^{M_x+1}\sum_{\ell=1}^{M_y+1}\tilde{\mathcal{F}}_n(t)\tilde{\mathcal{F}}_m(x)\tilde{\mathcal{F}}_\ell(y)\upsilon_{nm\ell},\tag{3.2}$$

or, in matrix-form

$$\psi(t_j,x_i)=\left(\tilde{\mathcal{F}}(t_j)\otimes\tilde{\mathcal{F}}(x_i)\right)\mathcal{V},\tag{3.3}$$

$$\psi(t_j,x_i,y_k)=\left(\tilde{\mathcal{F}}(t_j)\otimes\tilde{\mathcal{F}}(x_i)\otimes\tilde{\mathcal{F}}(y_k)\right)\mathcal{V},\tag{3.4}$$

where $\tilde{\mathcal{F}}_n(t)$, $\tilde{\mathcal{F}}_m(x)$, and $\tilde{\mathcal{F}}_\ell(y)$ are SVFPs, υ_{nm}, and $\upsilon_{nm\ell}$ are the unknown coefficients,

$$\tilde{\mathcal{F}}(t_j)=\left[\tilde{\mathcal{F}}_1(t_j),\tilde{\mathcal{F}}_2(t_j),\tilde{\mathcal{F}}_3(t_j),\dots,\tilde{\mathcal{F}}_{M_t}(t_j),\tilde{\mathcal{F}}_{M_t+1}(t_j)\right]^T,$$

$$\tilde{\mathcal{F}}(x_i)=\left[\tilde{\mathcal{F}}_1(x_i),\tilde{\mathcal{F}}_2(x_i),\tilde{\mathcal{F}}_3(x_i),\dots,\tilde{\mathcal{F}}_{M_x}(x_i),\tilde{\mathcal{F}}_{M_x+1}(x_i)\right]^T,$$

$$\tilde{\mathcal{F}}(y_k)=\left[\tilde{\mathcal{F}}_1(y_k),\tilde{\mathcal{F}}_2(y_k),\tilde{\mathcal{F}}_3(y_k),\dots,\tilde{\mathcal{F}}_{M_y}(y_k),\tilde{\mathcal{F}}_{M_y+1}(y_k)\right]^T,$$

$$\mathcal{V} = \left[\upsilon_{1,1}, \upsilon_{1,2}, \upsilon_{1,3}, \dots, \upsilon_{1,M_x+1}, \upsilon_{2,1}, \dots, \upsilon_{2,M_x+1}, \dots, \upsilon_{M_t+1,1}, \dots, \upsilon_{M_t+1,M_x+1}\right]^T,$$

for two variables, and

$$\mathcal{V} = \left[\upsilon_{1,1,1}, \upsilon_{1,1,2}, \dots, \upsilon_{1,1,M_y+1}, \upsilon_{1,2,1}, \dots, \upsilon_{1,2,M_y+1}, \dots, \upsilon_{1,M_x+1,1}, \dots, \upsilon_{1,M_x+1,M_y+1}, \upsilon_{2,1,1}, \dots, \upsilon_{M_t+1,M_x+1,M_y+1}\right]^T,$$

for three variables, and the symbol $\otimes$ represents the Kronecker-product of two matrices. If $A_{m\times n}$ matrix and $B_{p\times q}$ matrix, then $A\otimes B$ is the $(pm \times qn)$ matrix:

$$A\otimes B = \begin{bmatrix} a_{11}B & \cdots & a_{1n}B \\ \vdots & \ddots & \vdots \\ a_{m1}B & \cdots & a_{mn}B \end{bmatrix}.$$

The partial derivatives of $\psi(t,x)$ *w.r.t* x and t are defined by:

$$\frac{\partial^{q+p}}{\partial t^q \partial x^p}\psi(t,x) = \sum_{n=0}^{M_t+1}\sum_{m=1}^{M_x+1}\tilde{\mathcal{F}}_n^{(q)}(t)\tilde{\mathcal{F}}_m^{(p)}(x)\upsilon_{nm} = \left(D^{(q)}\tilde{\mathcal{F}}(t_j)\otimes D^{(p)}\tilde{\mathcal{F}}(x_i)\right)\mathcal{V}. \tag{3.5}$$

Moreover, the partial derivatives of $\psi(t,x,y)$ *w.r.t* x, y, and t are defined by:

$$\frac{\partial^{q+p+r}}{\partial t^q \partial x^p \partial y^r}\psi(t,x) = \sum_{n=0}^{M_t+1}\sum_{m=1}^{M_x+1}\sum_{\ell=1}^{M_y+1}\tilde{\mathcal{F}}_n^{(q)}(t)\tilde{\mathcal{F}}_m^{(p)}(x)\tilde{\mathcal{F}}_\ell^{(r)}(y)\upsilon_{nm\ell}$$

$$= \left(D^{(q)}\tilde{\mathcal{F}}(t_j)\otimes D^{(p)}\tilde{\mathcal{F}}(x_i)\otimes D^{(r)}\tilde{\mathcal{F}}(y_k)\right). \tag{3.6}$$

Additionally, the Brownian motion process $\mathcal{B}(t)$ and the white noise $n(t)$ should be defined using SVFPs. To achieve this in the stochastic setting, the Brownian motion $\mathcal{B}(t)$ is projected onto the SVFP basis to obtain a finite-dimensional surrogate suitable for spectral computation. Specifically, $\mathcal{B}(t)$ is approximated by

$$\mathcal{B}(t) = \sum_{n=1}^{M_t+1}\tilde{\mathcal{F}}_n(t)\mathfrak{b}_n,$$

$$\mathcal{B}(t_j) = \tilde{\mathcal{F}}(t_j)\mathfrak{B},\ j = 0,1,2,\dots,M_t,$$

$$\mathfrak{B} = \left[\tilde{\mathcal{F}}(t_j)\right]^{-1}\mathcal{B}(t_j), \tag{3.7}$$

where $\mathfrak{b}_n$ represents the unknown coefficients, $\mathfrak{B} = \left[\mathfrak{b}_1, \mathfrak{b}_2, \mathfrak{b}_3, \dots, \mathfrak{b}_{M_{t+1}}\right]^T$ and $\mathcal{B}(t)$ values are obtained from a built-in function in Mathematica software.

Since $n(t) = \mu\frac{d}{dt}\mathcal{B}(t)$, then

$$n(t) = \mu\sum_{n=1}^{M_t+1}D^{(1)}\tilde{\mathcal{F}}_n(t)\mathfrak{b}_n, \tag{3.8}$$

Hence, using the vector $\mathfrak{B}$ obtained by Eq (3.5), we can calculate the vector of $\mathcal{N}_w$ which represents the white-noise values at each level $j \geq 0$ as follows:

$$n(t_j) = \mu\left[D^{(1)}\tilde{\mathcal{F}}(t_j)\right]\mathfrak{B} \equiv \mathcal{N}_w. \tag{3.9}$$

This strategy mirrors standard spectral stochastic techniques, such as Fourier-based and polynomial-chaos representations, where the derivative of the projection, not the true Brownian path, is used for numerical approximation. Despite the inherently rough nature of Brownian motion, this projection-based formulation provides a stable and accurate stochastic forcing term for the SVFP solver.

3.2. Applying spectral approach to stochastic heat equations

The proposed technique can be applied to the SHE by substituting Eqs (3.3), (3.5), and (3.9) to SHE equations (1.1) and (1.2) at the point (t_j, x_i) as follows:

$$-\left(D^{(1)}\tilde{\mathcal{F}}(t_j)\otimes\tilde{\mathcal{F}}(x_i)\right)\mathcal{V} + \sigma\left(\tilde{\mathcal{F}}(t_j)\otimes D^{(2)}\tilde{\mathcal{F}}(x_i)\right)\mathcal{V}$$

$$+\varepsilon\left(\tilde{\mathcal{F}}(t_j)\otimes D^{(1)}\tilde{\mathcal{F}}(x_i)\right)\mathcal{V} + \rho(\mathcal{N}_w) * \left(\tilde{\mathcal{F}}(t_j)\otimes\tilde{\mathcal{F}}(x_i)\right)\mathcal{V} = 0, \tag{3.10}$$

and

$$-\left(D^{(1)}\tilde{\mathcal{F}}(t_j)\otimes\tilde{\mathcal{F}}(x_i)\right)\mathcal{V} + (\sigma)\left(\tilde{\mathcal{F}}(t_j)\otimes D^{(2)}\tilde{\mathcal{F}}(x_i)\right)\mathcal{V} + \rho(\mathcal{N}_w) * \left(\tilde{\mathcal{F}}(t_j)\otimes D^{(2)}\tilde{\mathcal{F}}(x_i)\right)\mathcal{V} = [\underline{\mathbf{0}}]. \tag{3.11}$$

Computing Eqs (3.10) and (3.11) for interior-grid point for $j = 1,2,3,\ldots,M_t$ and $i = 1,2,3,\ldots,M_x - 1$,

$$[-\left([\tilde{\mathcal{F}}_t]_{2:M_t+1}.D^{(1)}\otimes[\tilde{\mathcal{F}}_x]_{2:M_x}\right) + \sigma\left([\tilde{\mathcal{F}}_t]_{2:M_t+1}\otimes[\tilde{\mathcal{F}}_x]_{2:M_x}.D^{(2)}\right)$$

$$+\varepsilon\left([\tilde{\mathcal{F}}_t]_{2:M_t+1}\otimes[\tilde{\mathcal{F}}_x]_{2:M_x}.D^{(1)}\right) + \rho(\mathcal{N}_w)\circ\left([\tilde{\mathcal{F}}_t]_{2:M_t+1}\otimes[\tilde{\mathcal{F}}_x]_{2:M_x}\right)]\mathcal{V} = [\underline{\mathbf{0}}], \tag{3.12}$$

and

$$[-\left([\tilde{\mathcal{F}}_t]_{2:M_t+1}.D^{(1)}\otimes[\tilde{\mathcal{F}}_x]_{2:M_x}\right) + (\sigma)\left([\tilde{\mathcal{F}}_t]_{2:M_t+1}\otimes[\tilde{\mathcal{F}}_x]_{2:M_x}.D^{(2)}\right)$$

$$+\rho(\mathcal{N}_w)\circ\left([\tilde{\mathcal{F}}_t]_{2:M_t+1}\otimes[\tilde{\mathcal{F}}_x]_{2:M_x}.D^{(2)}\right)]\mathcal{V} = [\underline{\mathbf{0}}] \tag{3.13}$$

where $[\underline{\mathbf{0}}]$ represents a zero vector, the symbol $\circ$ denotes the Hadamard-product and $[\tilde{\mathcal{F}}_t]_{2:M_t+1}$, $[\tilde{\mathcal{F}}_x]_{2:M_x}$are submatrices of $\tilde{\mathcal{F}}_t$ and $\tilde{\mathcal{F}}_x$. $[\tilde{\mathcal{F}}_x]_{2:M_x}$ is a submatrix of rows $2:M_x$ and all columns of $\tilde{\mathcal{F}}_x$, the same for $[\tilde{\mathcal{F}}_t]_{2:M_t+1}$,

$$\tilde{\mathcal{F}}_x = \begin{bmatrix} \tilde{\mathcal{F}}_1(x_0) & \tilde{\mathcal{F}}_2(x_0) & \cdots & \tilde{\mathcal{F}}_{M_x}(x_0) & \tilde{\mathcal{F}}_{M_x+1}(x_0) \\ \tilde{\mathcal{F}}_1(x_1) & \tilde{\mathcal{F}}_2(x_1) & \cdots & \tilde{\mathcal{F}}_{M_x}(x_1) & \tilde{\mathcal{F}}_{M_x+1}(x_1) \\ \vdots & \vdots & \cdots & \vdots & \vdots \\ \tilde{\mathcal{F}}_1(x_{M_x}) & \tilde{\mathcal{F}}_2(x_{M_x}) & \cdots & \tilde{\mathcal{F}}_{M_x}(x_{M_x}) & \tilde{\mathcal{F}}_{M_x+1}(x_{M_x}) \end{bmatrix}^T,$$

and

$$\tilde{\mathcal{F}}_t = \begin{bmatrix} \tilde{\mathcal{F}}_1(t_0) & \tilde{\mathcal{F}}_2(t_0) & \cdots & \tilde{\mathcal{F}}_{M_t}(t_0) & \tilde{\mathcal{F}}_{M_t+1}(t_0) \\ \tilde{\mathcal{F}}_1(t_1) & \tilde{\mathcal{F}}_2(t_1) & \cdots & \tilde{\mathcal{F}}_{M_t}(t_1) & \tilde{\mathcal{F}}_{M_t+1}(t_1) \\ \vdots & \vdots & \cdots & \vdots & \vdots \\ \tilde{\mathcal{F}}_1(t_{M_t}) & \tilde{\mathcal{F}}_2(t_{M_t}) & \cdots & \tilde{\mathcal{F}}_{M_t}(t_{M_t}) & \tilde{\mathcal{F}}_{M_t+1}(t_{M_t}) \end{bmatrix}^T.$$

Applying the initial and boundary conditions (BCs) as follows:

1) $\psi(0, x_i) = \left(\tilde{\mathcal{F}}(0) \otimes \tilde{\mathcal{F}}(x_i)\right)\mathcal{V} = g(x_i)$, (initial condition)

$$\left([\tilde{\mathcal{F}}_t]_1 \otimes \tilde{\mathcal{F}}_x\right)\mathcal{V} = \left[g(x_0), g(x_1), \dots, g(x_{M_x})\right]^T, \tag{3.14}$$

2) $\psi(t_j, a) = \left(\tilde{\mathcal{F}}(t_j) \otimes \tilde{\mathcal{F}}(0)\right)\mathcal{V} = 0$, (left BCs)

$$\left(\tilde{\mathcal{F}}_t \otimes [\tilde{\mathcal{F}}_x]_1\right)\mathcal{V} = [\underline{\mathbf{0}}], \tag{3.15}$$

3) $\psi(t_j, b) = \left(\tilde{\mathcal{F}}(t_j) \otimes \tilde{\mathcal{F}}(a)\right)\mathcal{V} = 0$, (right BCs)

$$\left(\tilde{\mathcal{F}}_t \otimes [\tilde{\mathcal{F}}_x]_{M_x+1}\right)\mathcal{V} = [\underline{\mathbf{0}}]. \tag{3.16}$$

3.3. Applying spectral approach to multi-dimensional stochastic poisson equations

The proposed technique can be applied to the 2D and 3D stochastic poisson equations by substituting Eqs (3.2) and (3.3) to the Poisson equation (1.3) for $d = 2$ at the point (t_j, x_i) and for $d = 3$ at the point (t_j, x_i, y_k) as follows:

$$\left(D^{(2)}\tilde{\mathcal{F}}(t_j) \otimes \tilde{\mathcal{F}}(x_i)\right)\mathcal{V} + \left(\tilde{\mathcal{F}}(t_j) \otimes D^{(2)}\tilde{\mathcal{F}}(x_i)\right)\mathcal{V} + \rho(\mathcal{N}_w) = f(t_j, x_i), \text{ for } d = 2, \tag{3.17}$$

$$\left(D^{(2)}\tilde{\mathcal{F}}(t_j) \otimes \tilde{\mathcal{F}}(x_i) \otimes \tilde{\mathcal{F}}(y_k)\right)\mathcal{V} + \left(\tilde{\mathcal{F}}(t_j) \otimes D^{(2)}\tilde{\mathcal{F}}(x_i) \otimes \tilde{\mathcal{F}}(y_k)\right)\mathcal{V}$$

$$+ \left(\tilde{\mathcal{F}}(t_j) \otimes \tilde{\mathcal{F}}(x_i) \otimes D^{(2)}\tilde{\mathcal{F}}(y_k)\right)\mathcal{V} + \rho(\mathcal{N}_w) = f(t_j, x_i, y_k), \text{ for } d = 3. \tag{3.18}$$

Computing Eqs (3.17) and (3.18) at interior-grid point for $j = 1{:}\,M_t - 1,\ i = 1{:}\,M_x - 1$ and $k = 1{:}\,M_y - 1$,

$$\left[\left([\tilde{\mathcal{F}}_t]_{2:M_t}.D^{(2)}\otimes[\tilde{\mathcal{F}}_x]_{2:M_x}\right) + \left([\tilde{\mathcal{F}}_t]_{2:M_t}\otimes[\tilde{\mathcal{F}}_x]_{2:M_x}.D^{(2)}\right)\right]\mathcal{V}$$

$$= \left[[\mathbb{f}]_{1:M_x-1}^{1:M_t-1} - \rho(\mathcal{N}_w)\right]_{1\times(M_t-1)(M_x-1)}, \text{ for } d = 2, \tag{3.19}$$

$$\left[\left([\tilde{\mathcal{F}}_t]_{2:M_t}.D^{(2)}\otimes[\tilde{\mathcal{F}}_x]_{2:M_x}\otimes\left[\tilde{\mathcal{F}}_y\right]_{2:M_y}\right) + \left([\tilde{\mathcal{F}}_t]_{2:M_t}\otimes[\tilde{\mathcal{F}}_x]_{2:M_x}.D^{(2)}\otimes\left[\tilde{\mathcal{F}}_y\right]_{2:M_y}\right)\right.$$
$$\left. + \left([\tilde{\mathcal{F}}_t]_{2:M_t}\otimes[\tilde{\mathcal{F}}_x]_{2:M_x}\otimes\left[\tilde{\mathcal{F}}_y\right]_{2:M_y}.D^{(2)}\right)\right]\mathcal{V}$$
$$= \left[[\mathbb{f}]_{1:M_x-1;1:M_y-1}^{1:M_t-1} - \rho(\mathcal{N}_w)\right]_{1\times(M_t-1)(M_x-1)(M_y-1)}, \text{ for } d = 3, \tag{3.20}$$

where $[\mathbb{f}]_{1:M_x-1}^{1:M_t-1} = f(t_j, x_i)$, and $[\mathbb{f}]_{1:M_x-1;1:M_y-1}^{1:M_t-1} = f(t_j, x_i, y_k)$ are given column vectors.

Applying the BCs as follows:

- For 2D Poisson equation (4 BCs):

$$([\tilde{\mathcal{F}}_t]_1\otimes\tilde{\mathcal{F}}_x)\mathcal{V} = [\underline{\mathbf{0}}], \text{ for } t = a, \tag{3.21}$$

$$([\tilde{\mathcal{F}}_t]_{M_t+1}\otimes\tilde{\mathcal{F}}_x)\mathcal{V} = [\underline{\mathbf{0}}], \text{ for } t = b, \tag{3.22}$$

$$(\tilde{\mathcal{F}}_t\otimes[\tilde{\mathcal{F}}_x]_1)\mathcal{V} = [\underline{\mathbf{0}}], \text{ for } x = a, \tag{3.23}$$

$$(\tilde{\mathcal{F}}_t\otimes[\tilde{\mathcal{F}}_x]_{M_x+1})\mathcal{V} = [\underline{\mathbf{0}}] \text{for } x = b. \tag{3.24}$$

- For 3D Poisson equation (6 BCs):

$$([\tilde{\mathcal{F}}_t]_1\otimes\tilde{\mathcal{F}}_x\otimes\tilde{\mathcal{F}}_y)\mathcal{V} = [\underline{\mathbf{0}}] \text{for } t = a, \tag{3.25}$$

$$([\tilde{\mathcal{F}}_t]_{M_t+1}\otimes\tilde{\mathcal{F}}_x\otimes\tilde{\mathcal{F}}_y)\mathcal{V} = [\underline{\mathbf{0}}], \text{ for } t = b, \tag{3.26}$$

$$(\tilde{\mathcal{F}}_t\otimes[\tilde{\mathcal{F}}_x]_1\otimes\tilde{\mathcal{F}}_y)\mathcal{V} = [\underline{\mathbf{0}}], \text{ for } x = a, \tag{3.27}$$

$$(\tilde{\mathcal{F}}_t\otimes[\tilde{\mathcal{F}}_x]_{M_x+1}\otimes\tilde{\mathcal{F}}_y)\mathcal{V} = [\underline{\mathbf{0}}] \text{for } x = b, \tag{3.28}$$

$$\left(\tilde{\mathcal{F}}_t\otimes\tilde{\mathcal{F}}_x\otimes\left[\tilde{\mathcal{F}}_y\right]_1\right)\mathcal{V} = [\underline{\mathbf{0}}], \text{ for } y = a, \tag{3.29}$$

$$\left(\tilde{\mathcal{F}}_t \otimes \tilde{\mathcal{F}}_x \otimes \left[\tilde{\mathcal{F}}_y\right]_{M_y+1}\right)\mathcal{V} = [\underline{\mathbf{0}}], \text{ for } y = b. \tag{3.30}$$

3.4. Normalization matters: stabilizing solutions via orthonormal bases

In this part, we address the initial divergence issues encountered with raw SVFPs and introduce a normalization strategy to ensure stability. We redefine the basis functions and their derivatives in orthonormal form, significantly improving convergence and accuracy in stochastic simulations.

For the SHE, we solve the system of linear Eqs (3.12)–(3.16), which consists of $(M_x+1)(M_t+1)$ equations with $(M_x+1)(M_t+1)$ unknowns to get the values of the vector $\mathcal{V}$, and then substitute this into Eq (3.1) to get the numerical solutions of the SHE at all of the grid points. However, the resulting solutions are diverging. After many attempts, we successfully adddress this issue and achieve convergence by normalizing all vectors in the system. Assume the new orthonormal vectors are defined as:

$$\Phi_x = \frac{\tilde{\mathcal{F}}_x}{\mathcal{L}_{x,0}},\ D^{(1)}\Phi_x = \frac{D^{(1)}\cdot\tilde{\mathcal{F}}_x}{\mathcal{L}_{x,1}},\ D^{(2)}\Phi_x = \frac{D^{(2)}\cdot\tilde{\mathcal{F}}_x}{\mathcal{L}_{x,2}},\ \Phi_t = \frac{\tilde{\mathcal{F}}_t}{\mathcal{L}_{t,0}},$$

$$D^{(1)}\Phi_t = \frac{D^{(1)}\cdot\tilde{\mathcal{F}}_t}{\mathcal{L}_{t,1}},\ D^{(2)}\Phi_t = \frac{D^{(2)}\cdot\tilde{\mathcal{F}}_t}{\mathcal{L}_{t,2}},\ \Phi_y = \frac{\tilde{\mathcal{F}}_y}{\mathcal{L}_{y,0}}, \text{ and } D^{(2)}\Phi_y = \frac{D^{(2)}\cdot\tilde{\mathcal{F}}_y}{\mathcal{L}_{y,2}}, \tag{3.31}$$

where

$$\mathcal{L}_{x,0} = \left\|\tilde{\mathcal{F}}_x\right\|,\ \mathcal{L}_{x,1} = \left\|D^{(1)}\cdot\tilde{\mathcal{F}}_x\right\|,\ \mathcal{L}_{x,2} = \left\|D^{(2)}\cdot\tilde{\mathcal{F}}_x\right\|,\ \mathcal{L}_{t,0} = \left\|\tilde{\mathcal{F}}_t\right\|,$$
$$\mathcal{L}_{t,1} = \left\|D^{(1)}\cdot\tilde{\mathcal{F}}_t\right\|,\ \mathcal{L}_{y,0} = \left\|\tilde{\mathcal{F}}_y\right\|,\ \mathcal{L}_{y,2} = \left\|D^{(2)}\cdot\tilde{\mathcal{F}}_t\right\|,$$

and the symbol $\|.\|$ represents the infinity norm.

Applying these orthonormal vectors to the stochastic heat system of Eqs (3.12)–(3.16), we get

$$[-(\mathcal{L}_{t,1})\left(([\Phi_t]_{2:M_t+1}.D^{(1)})\otimes[\Phi_x]_{2:M_x}\right) + (\sigma\times\mathcal{L}_{x,2})\left([\Phi_t]_{2:M_t+1}\otimes([\Phi_x]_{2:M_x}.D^{(2)})\right)$$

$$+(\varepsilon\times\mathcal{L}_{x,1})\left([\Phi_t]_{2:M_t+1}\otimes([\Phi_x]_{2:M_x}.D^{(1)})\right) + \rho(\mathcal{N}_w)\circ([\Phi_t]_{2:M_t+1}\otimes[\Phi_x]_{2:M_x})]\mathcal{V} = [\underline{\mathbf{0}}], \tag{3.32}$$

or

$$[-(\mathcal{L}_{t,1})\left([\Phi_t]_{2:M_t+1}.(D^{(1)}\otimes[\Phi_x]_{2:M_x})\right) + (\sigma\times\mathcal{L}_{x,2})\left([\Phi_t]_{2:M_t+1}\otimes([\Phi_x]_{2:M_x}.D^{(2)})\right)$$

$$+(\rho\times\mathcal{L}_{x,2})(\mathcal{N}_w)\circ\left([\Phi_t]_{2:M_t+1}\otimes([\Phi_x]_{2:M_x}.D^{(2)})\right)]\mathcal{V} = [\underline{\mathbf{0}}], \tag{3.33}$$

with the initial and boundary conditions:

$$([\Phi_t]_1\otimes\Phi_x)\mathcal{V} = \left[g(x_0), g(x_1), \ldots, g\left(x_{M_x}\right)\right]^T, \tag{3.34}$$

$$(\Phi_t\otimes[\Phi_x]_1)\mathcal{V} = [\underline{\mathbf{0}}], \tag{3.35}$$

and

$$\left(\Phi_t \otimes [\Phi_x]_{M_x+1}\right)\mathcal{V} = [\underline{\mathbf{0}}]. \tag{3.36}$$

We determine the values of the vector $\mathcal{V}$ by solving the updated system of Eq (3.32) or Eq (3.33) with Eqs (3.34)–(3.36), and then use Eq (3.1) to get the proposed numerical solutions for the SHEs.

By the same manner for the SPEs, applying these orthonormal vectors to:

- Use the 2D Poisson system of Eqs (3.19) and (3.21)–(3.24), and we get

$$\left[\left(\mathcal{L}_{t,2}\right)\left([\Phi_t]_{2:M_t}.D^{(2)} \otimes [\Phi_x]_{2:M_x}\right) + \left(\mathcal{L}_{x,2}\right)\left([\Phi_t]_{2:M_t} \otimes [\Phi_x]_{2:M_x}.D^{(2)}\right)\right]\mathcal{V}$$

$$= \left[[\mathcal{F}]_{1:M_x-1}^{1:M_t-1} - \rho(\mathcal{N}_w)\right]_{1\times(M_t-1)(M_x-1)}, \tag{3.37}$$

$$([\Phi_t]_1 \otimes \Phi_x)\mathcal{V} = [\underline{\mathbf{0}}], \text{ for } t = a, \tag{3.38}$$

$$\left([\Phi_t]_{M_t+1} \otimes \Phi_x\right)\mathcal{V} = [\underline{\mathbf{0}}], \text{ for } t = b, \tag{3.39}$$

$$(\Phi_t \otimes [\Phi_x]_1)\mathcal{V} = [\underline{\mathbf{0}}], \text{ for } x = a, \tag{3.40}$$

$$\left(\Phi_t \otimes [\Phi_x]_{M_x+1}\right)\mathcal{V} = [\underline{\mathbf{0}}], \text{ for } x = b. \tag{3.41}$$

- To use the 3D Poisson system of Eqs (3.20) and (3.25)–(3.30), and we get

$$\left[\left(\mathcal{L}_{t,2}\right)\left([\Phi_t]_{2:M_t}.D^{(2)} \otimes [\Phi_x]_{2:M_x} \otimes \left[\Phi_y\right]_{2:M_y}\right) + \left(\mathcal{L}_{x,2}\right)\left([\Phi_t]_{2:M_t} \otimes [\Phi_x]_{2:M_x}.D^{(2)} \otimes \left[\Phi_y\right]_{2:M_y}\right)\right.$$

$$\left. + \left(\mathcal{L}_{y,2}\right)\left([\Phi_t]_{2:M_t} \otimes [\Phi_x]_{2:M_x} \otimes \left[\Phi_y\right]_{2:M_y}.D^{(2)}\right)\right]\mathcal{V}$$

$$= \left[[\mathcal{F}]_{1:M_x-1;1:M_y-1}^{1:M_t-1} - \rho(\mathcal{N}_w)\right]_{1\times(M_t-1)(M_x-1)(M_y-1)}, \tag{3.42}$$

$$\left([\Phi_t]_1 \otimes \Phi_x \otimes \Phi_y\right)\mathcal{V} = [\underline{\mathbf{0}}], \text{ for } t = a, \tag{3.43}$$

$$\left([\Phi_t]_{M_t+1} \otimes \Phi_x \otimes \Phi_y\right)\mathcal{V} = [\underline{\mathbf{0}}], \text{ for } t = b, \tag{3.44}$$

$$\left(\Phi_t \otimes [\Phi_x]_1 \otimes \Phi_y\right)\mathcal{V} = [\underline{\mathbf{0}}], \text{ for } x = a, \tag{3.45}$$

$$\left(\Phi_t \otimes [\Phi_x]_{M_x+1} \otimes \Phi_y\right)\mathcal{V} = [\underline{\mathbf{0}}], \text{ for } x = b, \tag{3.46}$$

$$\left(\Phi_t \otimes \Phi_x \otimes \left[\Phi_y\right]_1\right)\mathcal{V} = [\underline{\mathbf{0}}], \text{ for } y = a, \tag{3.47}$$

$$\left(\Phi_t \otimes \Phi_x \otimes \left[\Phi_y\right]_{M_y+1}\right)\mathcal{V} = [\underline{\mathbf{0}}], \text{ for } y = b. \tag{3.48}$$

We determine the values of the vector $\mathcal{V}$ by solving the updated linear system of Eqs (3.37)–(3.41) or Eqs (3.42)–(3.48) using matrix inversion or any other linear solver, and then use Eq (3.1) or Eq (3.2) to get the proposed numerical solutions for the 2D and 3D stochastic Poisson equations.

Finally, to handle the given stochastic equations, we need to utilize a variety of samples ($\mathcal{K} = 1, 2, 3, \dots$) of the Brownian motion (or, Wiener) process. Then, we solve this linear system for $\mathcal{K} = 1$ and redo the same procedure for $\mathcal{K} = 2, 3, 4, \dots$. Hence, we get the solution-sequences $\left\{\psi_{i,j}^{1}, \psi_{i,j}^{2}, \psi_{i,j}^{3}, \dots, \psi_{i,j}^{\mathcal{K}}\right\}$. Subsequently, we calculate the mean and variance of the resulting solutions to analyze the approximate solutions of the proposed stochastic Eqs (1.1)–(1.3).

The solution steps algorithm can be summarized as follows:

Step 1) Define all required parameters:

- Set grid sizes: M_x, M_t and M_y;
- Set domain limits: $a, b,$ and T;
- Define grid nodes: x_i, t_j, and y_k;
- Set the number of Monte-Carlo runs: $\mathcal{K}_{\text{runs}}$;
- Set the SPDE constants: σ, ε, and ρ;
- Set the SPDEs initial and boundary conditions.

Step 2) Generate basis functions (SVFPs):

- Initialize SVFPs basis functions and their derivatives: $\tilde{\mathcal{F}}(t_j)$, $\tilde{\mathcal{F}}(x_i)$, $\tilde{\mathcal{F}}(y_k)$, $D^{(q)}\tilde{\mathcal{F}}(t_j)$, $D^{(p)}\tilde{\mathcal{F}}(x_i)$, and $D^{(r)}\tilde{\mathcal{F}}(y_k)$, as defined in Eqs (2.6)–(2.10);
- Compute the basis functions and their derivatives on the grid points: $\tilde{\mathcal{F}}_x$, $D^{(1)}\tilde{\mathcal{F}}_x$, $D^{(2)}\tilde{\mathcal{F}}_x$, $\tilde{\mathcal{F}}_t$, $D^{(1)}\tilde{\mathcal{F}}_t$, $D^{(2)}\Phi_t$, $\tilde{\mathcal{F}}_y$, and $D^{(2)}\tilde{\mathcal{F}}_y$, as defined in Eqs (3.12)–(3.30);
- Normalize the basis functions and their derivatives on the grid points: Φ_x, $D^{(1)}\Phi_x$, $D^{(2)}\Phi_x$, Φ_t, $D^{(1)}\Phi_t$, $D^{(2)}\Phi_t$, Φ_y, and $D^{(2)}\Phi_y$, as defined in Eq (3.31).

Step 3) Generate noise realizations:

- Generate $\mathcal{K}$-paths of the Wiener Process on the time grid;
- Discretizing it with an equal step in time to get its value at each node j in time space;
- Generate the $\mathcal{B}(t)$ matrix and used it to get the vector of white noise $\mathcal{N}_w$, as illustrated in Eqs (3.7)–(3.9).

Step 4) Precompute system matrices:

- Construct the system matrices using Kronecker products of the basis function and their derivatives submatrices for the interior points: $[\Phi_x]_{2:M_x}$, $D^{(1)}\otimes[\Phi_x]_{2:M_x}$, $D^{(2)}\otimes[\Phi_x]_{2:M_x}$, $[\Phi_t]_{2:M_x}$, $D^{(1)}\otimes[\Phi_t]_{2:M_x}$, $D^{(2)}\otimes[\Phi_t]_{2:M_x}$, $\left[\Phi_y\right]_{2:M_x}$, and $D^{(2)}\otimes\left[\Phi_y\right]_{2:M_x}$, as defined in Eqs (3.32)–(3.48),
- Set up storage array to hold the solution vector for each $\mathcal{K}$.

Step 5) Monte Carlo simulation loop:

➢ *For* $\mathcal{K} = 1$ *to* $\mathcal{K}_{runs}$;

- Generate the white noise vector $\mathcal{N}_w$ for the current $\mathcal{K}$;
- Set the vector of unknown spectral coefficients;
- Formulate all matrices which represent the solution function and its derivatives using the required

Kronecker products of the defined matrices given in previous step;

- Formulate a set of linear algebraic equations at the interior grid points;
- Formulate a set of linear algebraic equations from the initial and boundary conditions;
- Combine the interior equations, initial equations and boundary equations, and solve it using matrix inversion to get the vector $\mathcal{V}$;
- Then, compute the full solution using Eq (3.1) or Eq (3.2);
- Store the current solution in the results array.

➢ *End For loop.*

Step 6) Computing the statistics:

- The numerical solutions across all $\mathcal{K}_{\text{runs}}$: $\psi^{(\mathcal{K})} = \left\{\psi_{i,j}^{1}, \psi_{i,j}^{2}, \psi_{i,j}^{3}, \ldots, \psi_{i,j}^{\mathcal{K}_{\text{runs}}}\right\}$;
- Calculate the Mean and Variance of the reconstructed solutions as follows:

$$\psi_{mean} = \frac{1}{\mathcal{K}_{\text{runs}}} \sum_{\mathcal{K}=1}^{\mathcal{K}_{\text{runs}}} \psi^{(\mathcal{K})}, \tag{3.49}$$

$$\psi_{var} = \frac{1}{\mathcal{K}_{\text{runs}}} \sum_{\mathcal{K}=1}^{\mathcal{K}_{\text{runs}}} \left(\psi^{(\mathcal{K})} - \psi_{mean}\right)^{2}. \tag{3.50}$$

4. Results

We validate the proposed method through numerical experiments on four benchmark problems for SHE and one benchmark problem for SPE, comparing absolute errors and convergence rates with the FDFT [7], TNPCS [8], Tau [28], Galerkin [28], and Quasi-Inverse Matrix Diagonalization (QIMD) [29] approaches. Tables and contour plots illustrate the superior precision of SVFPs, particularly for problems with exact solutions.

We set the spatial and temporal discretization parameters to $M = 16$ and employ 2000 samples of the Brownian motion $\mathcal{B}(t)$. The mean of the solutions and the variance under the influence of noise for four SHEs are illustrated and visualized in Figures 1–4. For the multi-dimensional SPE, we configure discretization parameters to $M = 16$ across all dimensions, yielding high-accuracy solutions. The results are shown in Figures 5 and 6 and are detailed in Tables 3 and 4.

The visual representations highlight the robustness of our orthonormal SVFPs method in effectively addressing and managing stochastic variability. Using Monte Carlo samples of Brownian motion, we analyze the variance of SVFP solutions against competing methods. Our results demonstrate that SVFPs achieve orders-of-magnitude lower variance, highlighting their robustness to stochastic fluctuations.

Tables 1–4 present a quantitative comparison of absolute errors obtained via the FDFT method, literature approaches, and our approach. These tables redemonstrate that our proposed method reduces computational time and resource requirements with a high-level of accuracy.

In [7], the authors demonstrated that the solutions obtained using the FDFT method are more reliable than those derived from the stochastic TNPCS approach [8]. In this work, we compare the proposed approach, based on SVFPs, with the FDFT method. The results show that the proposed approach achieves greater reliability and efficiency, as evidenced by the lower variance in the solutions compared to those obtained by the FDFT method.

By increasing the number of samples of the noise term, our SVFPs approach demonstrates unwavering reliability, consistently yielding robust results across all analyzed problems. All

computations are executed by *Mathematica 12* software, ensuring an environment of reliability for our analysis.

Table 1. The absolute errors of problem (3) at $t = 1$.

x	Exact	Errors by SVFPs		Errors by FDFT [7]
		$\rho = 0$	$\rho = 0.01$	$\rho = 0$
0.125	0.140781367244039	5.254×10^{-12}	1.767×10^{-10}	1.173×10^{-6}
0.250	0.260130047511444	4.458×10^{-12}	3.262×10^{-10}	2.167×10^{-6}
0.375	0.339876286129985	7.198×10^{-12}	4.262×10^{-10}	2.832×10^{-6}
0.500	0.36787944117144	7.559×10^{-12}	4.613×10^{-10}	3.066×10^{-6}
0.625	0.339876286129985	7.198×10^{-12}	4.262×10^{-10}	2.832×10^{-6}
0.750	0.260130047511444	5.254×10^{-12}	3.262×10^{-10}	2.167×10^{-6}
0.875	0.140781367244039	4.458×10^{-12}	1.767×10^{-10}	1.173×10^{-6}
1.000	0	0	0	0

Table 2. The absolute errors of problem (4) at $t = 1$.

x	Exact	Errors by SVFPs		Errors by FDFT [7]
		$\rho = 0$	$\rho = 0.01$	$\rho = 0$
0.125	0.095696496510411	1.025×10^{-9}	4.965×10^{-9}	1.173×10^{-6}
0.250	0.135335283236612	8.991×10^{-10}	6.476×10^{-9}	2.167×10^{-6}
0.375	0.095696496510411	5.038×10^{-10}	4.447×10^{-9}	2.832×10^{-6}
0.500	0	0	0	3.066×10^{-6}
0.625	-0.095696496510411	5.038×10^{-10}	4.447×10^{-9}	2.832×10^{-6}
0.750	-0.135335283236612	8.991×10^{-10}	6.476×10^{-9}	2.167×10^{-6}
0.875	-0.095696496510411	1.025×10^{-9}	4.965×10^{-9}	1.173×10^{-6}
1.000	0	0	0	0

Table 3. The maximum absolute errors of problem (5) related to 2D and 3D SPE.

Method	M	E_{max} (2D)	E_{max} (3D)
SVFPs	16	5.75×10^{-4}	3.33×10^{-4}
	32	1.39×10^{-15}	1.28×10^{-15}
FDFT [7]	16	7.41×10^{-5}	7.41×10^{-5}
	32	1.12×10^{-6}	1.12×10^{-6}
Tau [28]	16	1.45×10^{-6}	1.34×10^{-6}
	32	1.55×10^{-15}	4.62×10^{-15}
Galerkin [28]	16	6.37×10^{-6}	8.32×10^{-6}
	32	1.41×10^{-15}	9.2×10^{-15}

Table 4. The relative L2-norm errors of problem (5) related to 2D and 3D SPE.

Method	M	RL_2 error (2D)	RL_2 error (3D)
SVFPs	16	4.71×10^{-4}	2.28×10^{-4}
	32	1.18×10^{-15}	$1..12 \times 10^{-15}$
FDFT [7]	16	7.40×10^{-5}	7.40×10^{-5}
	32	1.13×10^{-6}	1.13×10^{-6}
QIMD [29]	16	1.75×10^{-6}	2.83×10^{-7}
	32	1.43×10^{-15}	3.62×10^{-15}

Problem (1). Recognize the initial-boundary value problem [8].

$$\frac{\partial}{\partial t}\psi(t,x) = 0.01\frac{\partial^2}{\partial x^2}\psi(t,x) + 0.01\frac{\partial}{\partial x}\psi(t,x) - 0.02\psi(t,x)n(t),$$

$$\psi(0,x) = x^2(1-x)^2,\ x \in [0,1],$$

$$\psi(t,0) = \psi(t,1) = 0,\ t \in [0,0.3].$$

Problem (2). Consider the stochastic PDE [8].

$$\frac{\partial}{\partial t}\psi(t,x) = \frac{\partial^2}{\partial x^2}\psi(t,x) - 0.01\,\psi(t,x)\,n(t),$$

$$\psi(0,x) = \sin(\pi x),\ x \in [0,1],$$

$$\psi(t,0) = \psi(t,1) = 0,\ t \in [0,0.3].$$

The mean results, its contour plots, and the variance for problems (1) and (2) are obtained using the SVFP approach and visualized in Figures 1 and 2. The SVFP method achieves a variance of solutions in the order of $O(10^{-11})$ in problem (1), and $O(10^{-9})$ in problem (2), demonstrating superior accuracy compared to the solutions obtained via FDFT.

Problem (3). Recognize the linear stochastic equation [7,8].

$$\frac{\partial}{\partial t}\psi(t,x) = \left(\frac{1}{\pi^2} + 0.01\,n(t)\right)\frac{\partial^2}{\partial x^2}\psi(t,x),$$

$$\psi(0,x) = \sin(\pi x),\ x \in [0,1],$$

$$\psi(t,0) = \psi(t,1) = 0,\ t \in [0,1],$$

and the exact solution for $\beta = 0$ is: $\psi(t,x) = e^{-t}\sin(\pi x)$.

Problem (4). Let the stochastic equation [7,8].

$$\frac{\partial}{\partial t}\psi(t,x) = \left(\frac{1}{2\pi^2} + 0.01\,n(t)\right)\frac{\partial^2}{\partial x^2}\psi(t,x),$$

$$\psi(t,0) = \sin(2\pi x),\ x \in [0,1],$$

$$\psi(t,0) = \psi(t,1) = 0,\ t \in [0,1],$$

and the exact solution for $\beta = 0$ is: $\psi(t,x) = e^{-2t}\sin(2\pi x)$.

The solution and absolute errors for problems (3) and (4), with noise term coefficients $\rho = 0$ and $\rho = 0.01$, are presented in Tables 1 and 2, confirming the high accuracy of our approach. Additionally, the mean results, its contour plots, and the variance for these problems, are visualized in Figures 3 and 4. This method achieves a variance of solutions in the order of $O(10^{-15})$ in problem (3), and $O(10^{-11})$ in problem (4), significantly outperforming the FDFT method, as evidenced by the comparative results shown in the figures.

Problem (5). Consider the muti-dimensional SPE (1.3) with $[a,b] = [-1,1]$ and in the absence of noise, $f(\boldsymbol{x}) = -d(4\pi^2)\prod_{l=1}^{d}\sin(2\pi \boldsymbol{x_l})$.

In Tables 3 and 4, the accuracy of the solutions is evaluated using SVFPs, FDFT [8], Tau [28], Galerkin [28], and QIMD [29] methods for $\rho = 0$, $M = 16$, and 32. To assess the accuracy of the proposed numerical scheme, we compute the maximum absolute error, which quantifies the largest pointwise deviation between the numerical approximation and the exact solution. It is defined as:

$$E_{max} = max_i|\psi_{exact}(t_i) - \psi_{num}(t_i)|.$$

Additionally, we compute the relative L2-norm error, which is defined as: $\mathrm{RL}_2\mathrm{Error} = \frac{\|u_{\mathrm{numerical}} - u_{\mathrm{exact}}\|_2}{\|u_{\mathrm{exact}}\|_2}$.

These metrics provide a clear measure of the method's performance across the computational domain, and they are used in the tables to compare the accuracy of the schemes.

Furthermore, for $\rho = 0.01$, the mean and variance of solutions for 2D and 3D SPEs across different values of y are presented in Figures 5 and 6. These results validate the effectiveness of the proposed technique in multi-dimensional stochastic domains.

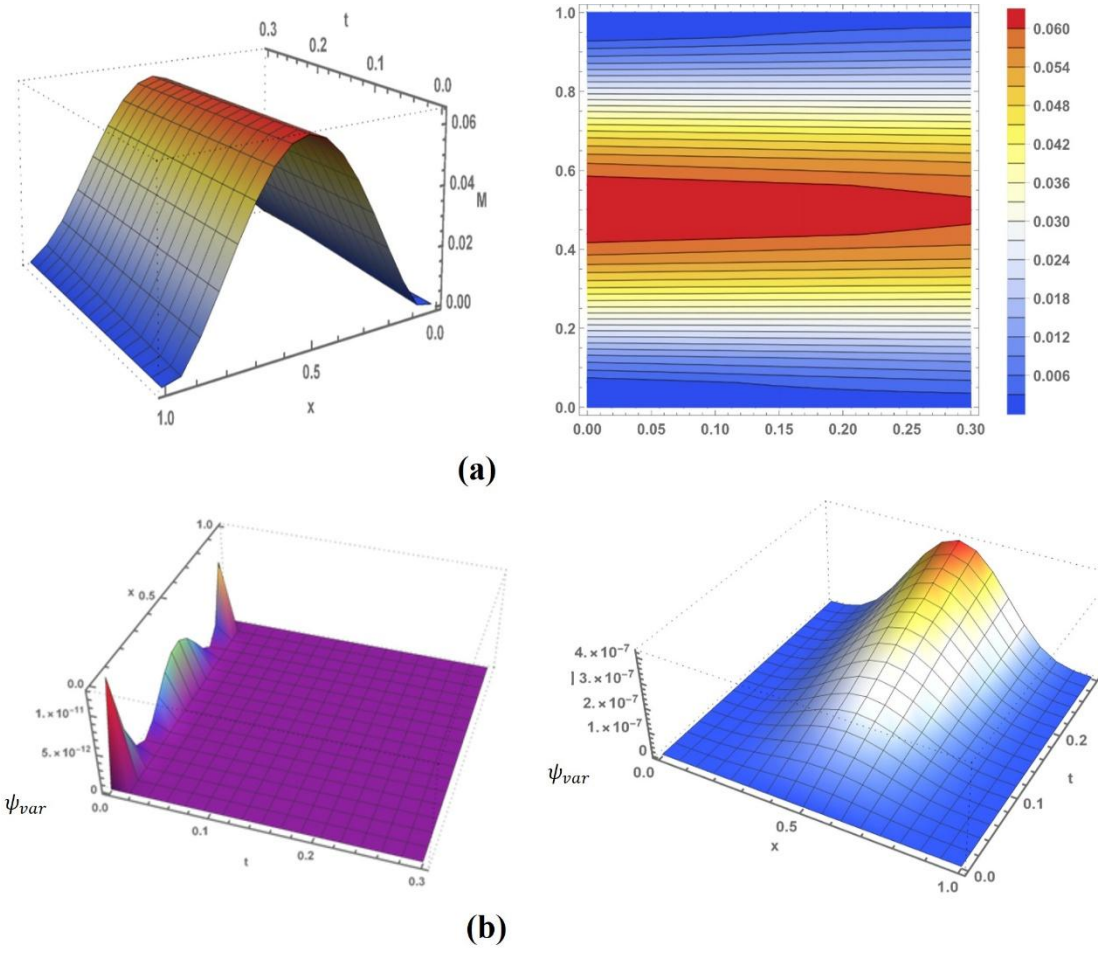

Figure 1. Spatial profile of the mean field and variance field for the solution of the stochastic heat equation (Problem 1), with stochastic forcing intensity $\rho = 0.01$: **(a)** mean field and its contour plot, and the variance field given by **(b)** SVFPs and **(c)** FDFT.

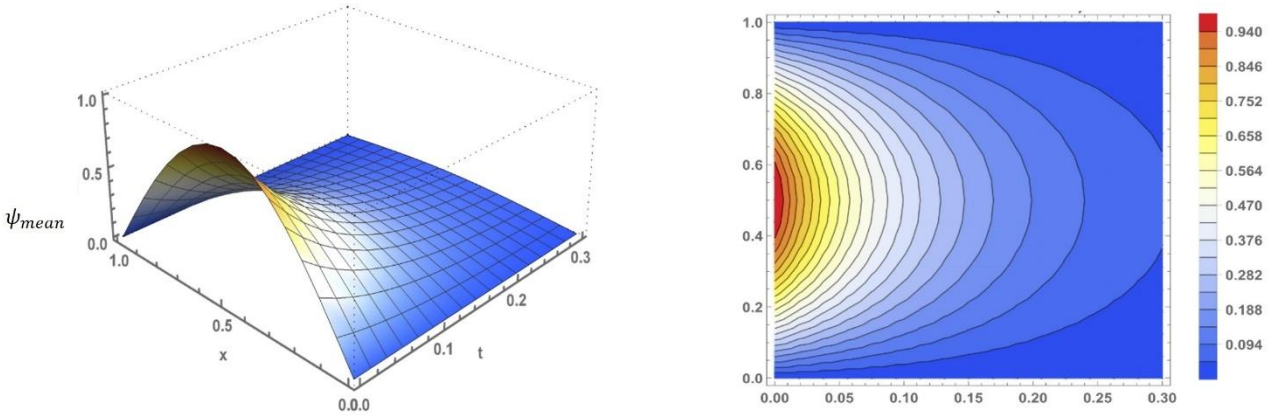

(a)

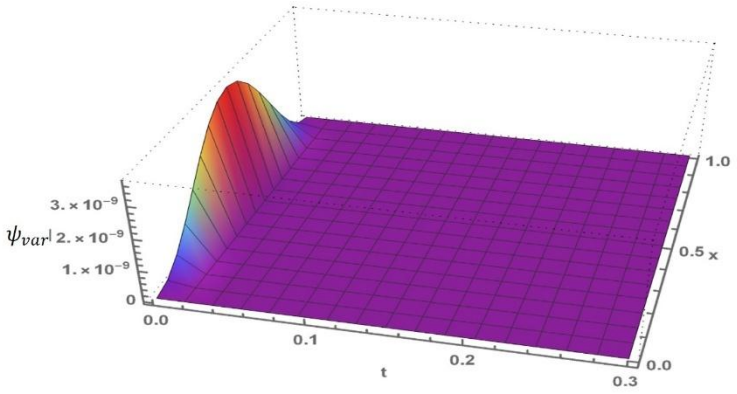

(b)

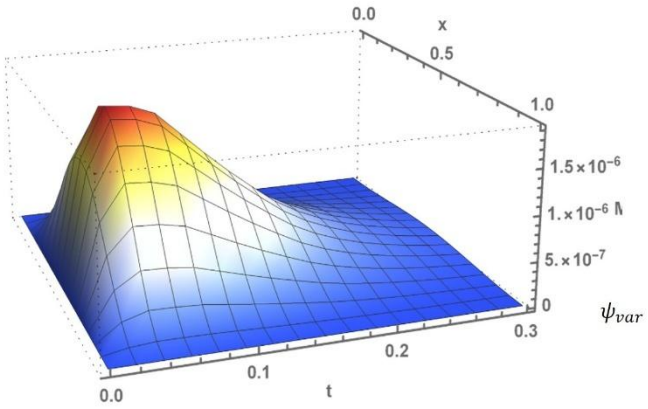

(c)

Figure 2. Spatial profile of the mean field and variance field for the solution of the stochastic heat equation (Problem 2), with stochastic forcing intensity $\rho = 0.01$: **(a)** mean field and its contour plot, and the variance field given by **(b)** SVFPs and **(c)** FDFT.

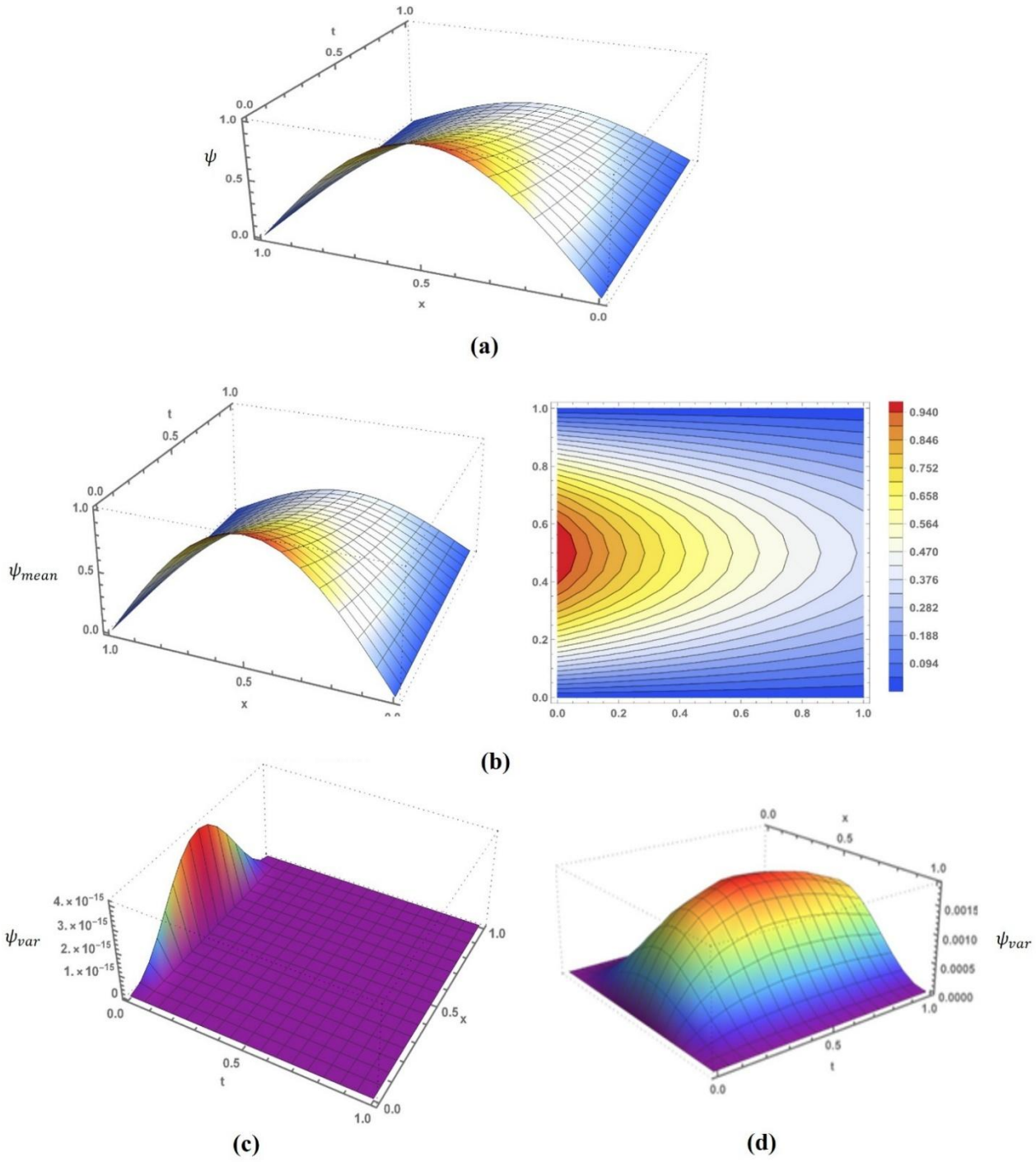

Figure 3. Spatial profile of the mean field and variance field for the solution of the stochastic heat equation (Problem 3), with stochastic forcing intensity $\rho = 0.01$: **(a)** exact solution $(\rho = 0)$, **(b)** mean field and its contour plot, and the variance field given by **(c)** SVFPs and **(d)** FDFT.

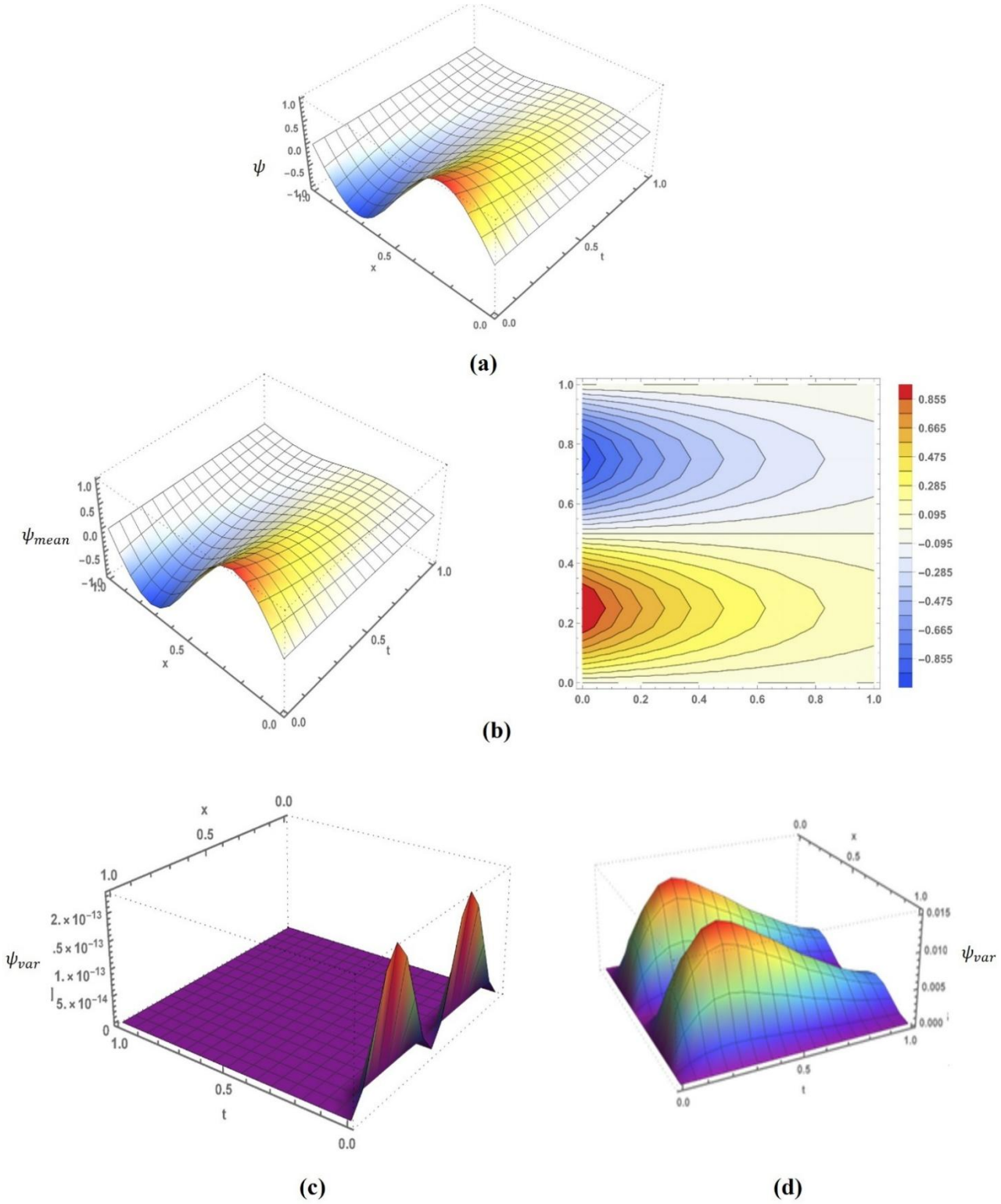

Figure 4. Spatial profile of the mean field and variance field for the solution of the stochastic heat equation (Problem 4), with stochastic forcing intensity $\rho = 0.01$: **(a)** exact solution $(\rho = 0)$, **(b)** mean field and its contour plot, and the variance field given by **(c)** SVFPs and **(d)** FDFT.

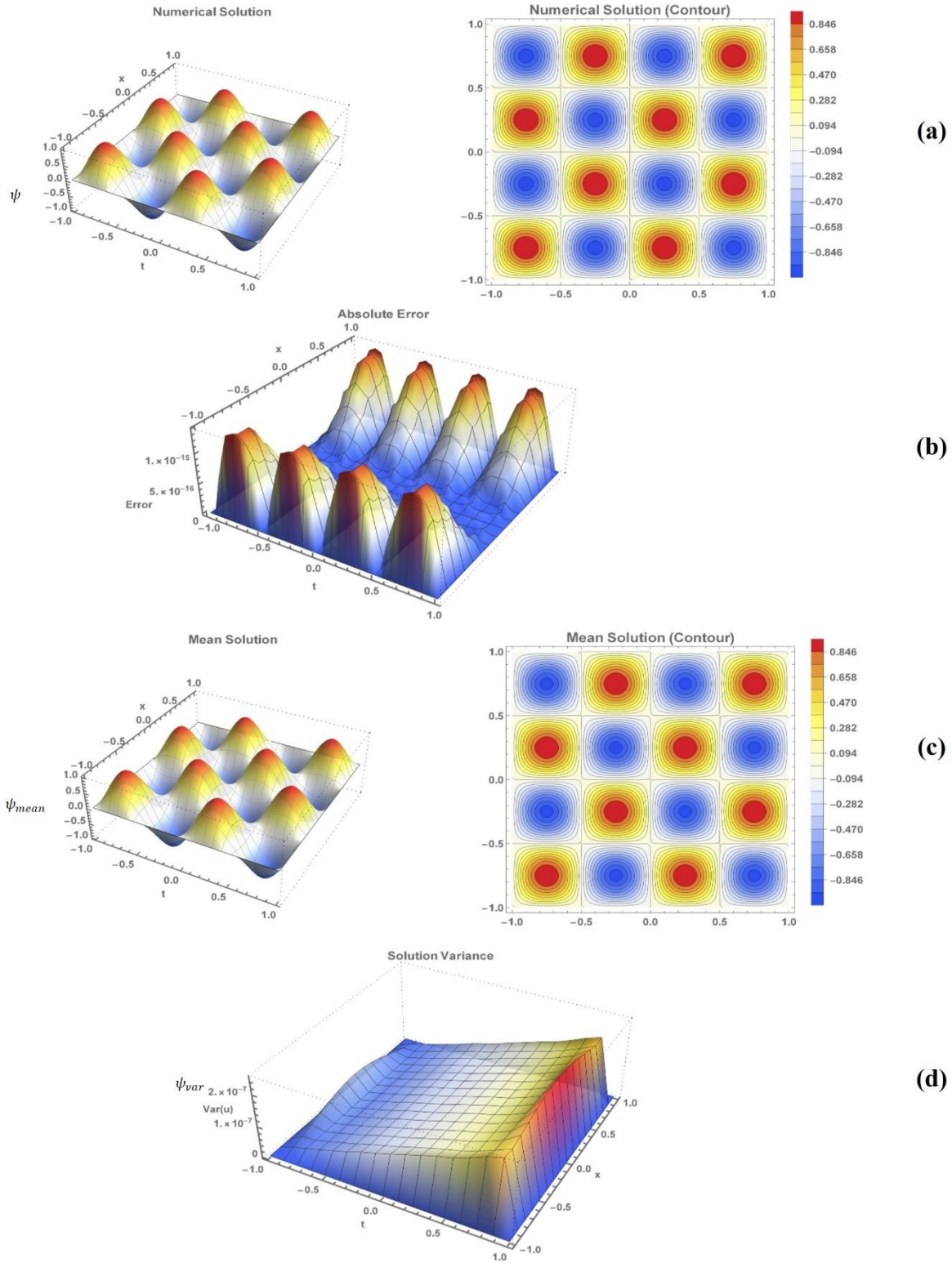

Figure 5. The numerical simulation of the 2D deterministic Poisson equation (Problem 5): **(a)** approximated solution and its contour plot and **(b)** absolute error of the solutions, and the spatial profile of the mean field and variance field of its stochastic version with a stochastic forcing intensity $\rho = 0.01$: **(c)** mean field and its contour plot and **(d)** variance field given by SVFPs.

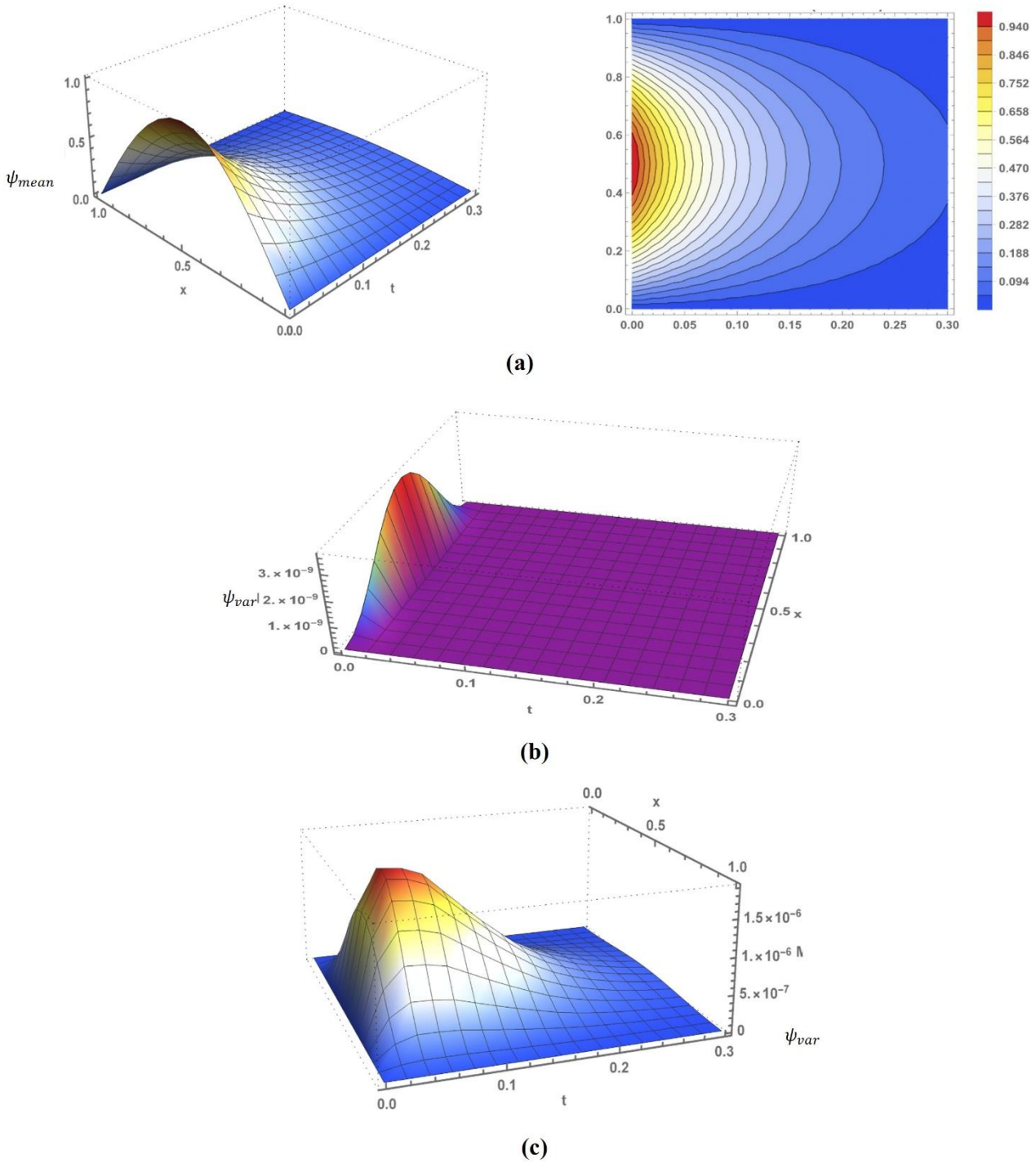

Figure 6. Spatial profile of the mean field and variance field for the solution of the three-dimensional stochastic Poisson equation (Problem 5) at different values of the spatial coordinate y, with stochastic forcing intensity $\rho = 0.01$. The mean field represents the expected solution, while the variance quantifies the uncertainty around this mean due to the stochastic source term.

5. Discussion and conclusions

5.1. Discussion

The numerical experiments conducted in this study reveal several important insights about the behavior and performance of SVFPs in solving stochastic equations. Three key findings emerge from the analysis that warrant careful consideration.

First, the spectral convergence properties of SVFPs demonstrate clear advantages over traditional finite difference methods. As shown in Tables 2–5, the SVFP approach achieves significantly smaller absolute errors compared to FDFT, TNPCS, Tau, Galerkin, and QIMD methods across all test cases. This superior accuracy can be attributed to the inherent properties of orthogonal polynomial expansions, which provide exponential convergence rates for smooth solutions. The normalization procedure developed in Section 3.2 proves particularly effective in maintaining this high accuracy while preventing the ill-conditioning issues that often plague high-order polynomial methods.

Second, the variance analysis presented in Figures 1–6 reveals the method's robustness in handling stochastic perturbations. The SVFP solutions exhibit consistently lower variance compared to FDFT results, suggesting greater stability in the presence of noise. This improved performance stems from the method's ability to represent the stochastic terms through orthogonal expansions rather than finite difference approximations, thereby reducing spurious oscillations and numerical artifacts.

However, several practical considerations must be noted regarding computational implementation. While the SVFP method requires more extensive pre-processing for matrix assembly compared to finite difference schemes, this initial investment pays dividends in long-time simulations. The method's memory requirements grow quadratically with the number of basis functions, which may limit its immediate some application to very high-order muti-dimensional problems. In future work, researchers could explore sparse implementations or adaptive basis selection to mitigate these scaling challenges.

This study leaves open several promising directions for future research. Extending the method to nonlinear stochastic PDEs would require developing appropriate linearization techniques while preserving the favorable convergence properties. Additionally, investigating time-adaptive versions of the algorithm could further improve computational efficiency for problems with multiple temporal scales. The potential combination of SVFPs with reduced-order modeling techniques presents another interesting avenue for handling multi-dimensional stochastic systems.

The numerical outcomes provide a direct physical interpretation of stochastic diffusion processes. The obtained mean solution represents the expected field, such as the average temperature distribution in a stochastic heat transfer problem, while the computed variance quantifies the spatial map of uncertainty around this mean arising from random forcing or material fluctuations. The observed decay and smooth distribution of variance with increased resolution reflect a fundamental property of diffusive systems: The natural damping of high-frequency stochastic noise, leading to more predictable macroscopic behavior. This characterization of uncertainty is vital for risk-aware engineering as regions of concentrated variance highlight system sensitivities critical for robust design and reliability analysis.

While the numerical results demonstrate the high accuracy and stability of the SVFPs method for SPDEs, we evaluate the combined error from the spectral discretization and Monte Carlo sampling. A formal convergence analysis separating these error components, along with a detailed study of

convergence rates in polynomial degree and number of stochastic trajectories, represents a valuable direction for future research. Such a study would provide further theoretical underpinning and is planned as a separate, detailed investigation.

These results collectively suggest that SVFPs offer a viable alternative to numerical methods for stochastic PDEs, particularly in scenarios where high accuracy and noise robustness are prioritized. The method's strong theoretical foundation and promising numerical performance establishes it as a valuable addition to the computational mathematician's toolkit for stochastic problems. Further development of the technique may open new possibilities for solving challenging problems in stochastic modeling and uncertainty quantification.

5.2. Conclusions

This investigation represents the inaugural implementation of SVFPs for stochastic PDEs, marking a significant departure from conventional numerical approaches. The developed methodology demonstrates three principal advancements: First, it establishes SVFPs as viable basis functions for stochastic systems; second, it introduces a stabilization protocol that preserves spectral accuracy while mitigating noise amplification; and third, it provides a framework for orthogonal polynomial expansions in stochastic settings that maintains superior accuracy.

The demonstrated success of this approach suggests several meaningful extensions that would broaden its applicability while maintaining mathematical rigor. A logical progression involves generalization to spatially extended systems, where the inherent tensor-product structure of polynomial bases could be judiciously employed to balance accuracy with dimensionality constraints. Such extension would necessitate careful consideration of basis selection strategies to maintain numerical stability in higher dimensions.

Furthermore, the incorporation of fractional calculus operators presents an opportunity to model non-local diffusion processes while preserving the method's convergence properties. This extension would be particularly relevant for systems exhibiting anomalous transport characteristics, where traditional approaches often struggle with accuracy preservation. The polynomial structure of SVFPs appears naturally compatible with such generalizations, given their established performance in fractional-order problems.

The method's novel application to stochastic systems also motivates investigation of more sophisticated noise models. In future work, researchers should examine correlated noise structures and state-dependent stochasticity, which would require development of weighted polynomial expansions or hybrid numerical-analytical approaches. These extensions would substantially broaden the method's applicability to real-world systems where noise characteristics deviate from idealized white noise assumptions.

From an implementation perspective, adaptive refinement strategies could enhance the method's efficiency for problems with localized features or multiple scales. The development of such adaptive schemes would build upon the method's inherent accuracy while addressing potential computational bottlenecks in complex applications.

In this work, we establish SVFPs as a new computational tool for stochastic systems, with demonstrated advantages in accuracy and stability. Its successful application to stochastic heat and stochastic Poisson equations suggests broader potential in areas requiring precise stochastic modeling, while the outlined extensions point toward meaningful future developments in numerical analysis for

stochastic systems. The methodology's novelty lies not only in its implementation but also in its potential to inspire new approaches to stochastic computation through orthogonal polynomial expansions.

Author contributions

A.G.K.: Conceptualization, supervision, investigation, validation, mathematical analysis, writing the original draft, and formal analysis. D.A.H.: Investigation, validation, writing review, and editing. M.S.S.: Mathematical analysis, validation, formal analysis, writing review, and editing. E.A.M: Investigation, validation, formal analysis, and editing. I.M.: Investigation and validation. A.F.F.: Formal analysis, investigation, literature review, writing review, and editing. All authors have read and agreed to the published version of the manuscript.

Use of Generative-AI tools declaration

The authors declare they have not used Artificial Intelligence (AI) tools in the creation of this article.

Acknowledgments

The authors extend their appreciation to Prince Sattam bin Abdulaziz University for funding this research work through the project number (PSAU/2025/01/34567).

Conflict of interest

The authors declare no conflicts of interest in this paper.

References

1. B. Øksendal, *Stochastic differential equations: an introduction with applications*, Springer, 2003. https://doi.org/10.1007/978-3-642-14394-6
2. G. Da Prato, J. Zabczyk, *Stochastic equations in infinite dimensions*, 2 Eds., Cambridge University Press, 2014.
3. L. Gorelick, M. Galun, E. Sharon, R. Basri, A. Brandt, Shape representation and classification using the poisson equation, *IEEE Trans. Pattern Anal. Mach. Intell.*, **28** (2006), 1991–2005. https://doi.org/10.1109/TPAMI.2006.253
4. A. Frckowiak, J. V. Wolfersdorf, M. Ciałkowski, Solution of the inverse heat conduction problem described by the Poisson equation for a cooled gas-turbine blade, *Int. J. Heat Mass Transf.*, **54** (2011), 1236–1243. https://doi.org/10.1016/j.ijheatmasstransfer.2010.11.001
5. C. Dick, M. Rogowsky, R. Westermann, Solving the fluid pressure poisson equation using multigrid– evaluation and improvements, *IEEE Trans. Vis. Comput. Graph.*, **22** (2016), 2480–2492. https://doi.org/10.1109/TVCG.2015.2511734
6. P. Koehl, Electrostatics calculations: latest methodological advances, *Curr. Opin. Struct. Biol.*, **16** (2006), 142–151. https://doi.org/10.1016/j.sbi.2006.03.001

7. A. G. Khattab, M. S. Semary, D. A. Hammad, A. F. Fareed, Exploring stochastic heat equations: a numerical analysis with fast discrete fourier transform techniques, *Axioms*, **13** (2024), 886. https://doi.org/10.3390/axioms13120886
8. A. F. Fareed, A. G. Khattab, M. S. Semary, A novel stochastic ten non-polynomial cubic splines method for heat equations with noise term, *Partial Differ. Equations Appl. Math.*, **10** (2024), 100677. https://doi.org/10.1016/j.padiff.2024.100677
9. D. A. Hammad, M. S. Semary, A. G. Khattab, Ten non-polynomial cubic splines for some classes of Fredholm integral equations, *Ain Shams Eng. J.*, **13** (2022), 101666. https://doi.org/10.1016/j.asej.2021.101666
10. D. Uma, H. Jafari, S. Raja Balachandar, S. G. Venkatesh, An approximation method for stochastic heat equation driven by white noise, *Int. J. Appl. Comput. Math.*, **8** (2022), 274. https://doi.org/10.1007/s40819-022-01376-4
11. A. Nouy, Recent developments in spectral stochastic methods for the numerical solution of stochastic partial differential equations, *Arch. Comput. Methods Eng.*, **16** (2009), 251–285. https://doi.org/10.1007/s11831-009-9034-5
12. R. Anton, D. Cohen, L. Quer-Sardanyons, A fully discrete approximation of the one-dimensional stochastic heat equation, *IMA J. Numer. Anal.*, **40** (2020), 247–284. https://doi.org/10.1093/imanum/dry060
13. Y. H. Youssri, M. M. Muttardi, A mingled tau-finite difference method for stochastic first-order partial differential equations, *Int. J. Appl. Comput. Math.*, **9** (2023), 14. https://doi.org/10.1007/s40819-023-01489-4
14. M. Gerencsér, I. Gyöngy, Finite difference schemes for stochastic partial differential equations in Sobolev spaces, *Appl. Math. Optim.*, **72** (2015), 77–100. https://doi.org/10.1007/s00245-014-9272-2
15. I. Masti, K. Sayevand, On collocation-Galerkin method and fractional B-spline functions for a class of stochastic fractional integro-differential equations, *Math. Comput. Simul.*, **216** (2024), 263–287. https://doi.org/10.1016/j.matcom.2023.09.013
16. A. F. Fareed, M. S. Semary, Stochastic improved Simpson for solving nonlinear fractional-order systems using product integration rules, *Nonlinear Eng.*, **14** (2025), 20240070. https://doi.org/10.1515/nleng-2024-0070
17. A. F. Fareed, E. A. Mohamed, M. Aly, M. S. Semary, A novel numerical method for stochastic conformable fractional differential systems, *AIMS Math.*, **10** (2025), 7509–7525. https://doi.org/10.3934/math.2025345
18. A. F. Fareed, E. A. Mohamed, A. Mokhtar, M. S. Semary, A novel fractional integral transform-based homotopy perturbation method for some nonlinear differential systems, *Fractal Fract.*, **9** (2025), 212. https://doi.org/10.3390/fractalfract9040212
19. F. Mirzaee, S. Rezaei, N. Samadyar, Numerical solution of two-dimensional stochastic time-fractional Sine–Gordon equation on non-rectangular domains using finite difference and meshfree methods, *Eng. Anal. Bound. Elem.*, **127** (2021), 53–63. https://doi.org/10.1016/j.enganabound.2021.03.009
20. R. Sharma, Rajeev, A numerical approach based on Vieta–Fibonacci polynomials to solve fractional order advection–reaction diffusion problem, *J. Anal.*, **33** (2025), 1251–1275. https://doi.org/10.1007/s41478-024-00804-6

21. A. Moumen, A. Mennouni, M. Bouye, A novel Vieta–Fibonacci projection method for solving a system of fractional integrodifferential equations, *Mathematics*, **11** (2023), 3985. https://doi.org/10.3390/math11183985
22. S. M. Sivalingam, P. Kumar, V. Govindaraj, R. A. Qahiti, W. Hamali, Z. M. Mutum, An operational matrix approach with Vieta-Fibonacci polynomial for solving generalized Caputo fractal-fractional differential equations, *Ain Shams Eng. J.*, **15** (2024), 102678. https://doi.org/10.1016/j.asej.2024.102678
23. H. Azin, M. H. Heydari, F. Mohammadi, Vieta–Fibonacci wavelets: application in solving fractional pantograph equations, *Math. Methods Appl. Sci.*, **45** (2022), 411–422. https://doi.org/10.1002/mma.7783
24. K. Sadri, K. Hosseini, D. Baleanu, S. Salahshour, C. Park, Designing a matrix collocation method for fractional delay integro-differential equations with weakly singular kernels based on vieta–fibonacci polynomials, *Fractal Fract.*, **6** (2022), 2. https://doi.org/10.3390/fractalfract6010002
25. P. Agarwal, A. A. El-Sayed, J. Tariboon, Vieta–Fibonacci operational matrices for spectral solutions of variable-order fractional integro-differential equations, *J. Comput. Appl. Math.*, **382** (2021), 113063. https://doi.org/10.1016/j.cam.2020.113063
26. M. H. Heydari, Z. Avazzadeh, A. Atangana, Shifted Vieta-Fibonacci polynomials for the fractal-fractional fifth-order KdV equation, *Math. Methods Appl. Sci.*, **44** (2021), 6716–6730. https://doi.org/10.1002/mma.7219
27. Z. Abbasi, M. Izadi, M. M. Hosseini, A highly accurate matrix method for solving a class of strongly nonlinear BVP arising in modeling of human shape corneal, *Math. Methods Appl. Sci.*, **46** (2023), 1511–1527. https://doi.org/10.1002/mma.8592
28. K. Julien, M. Watson, Efficient multi-dimensional solution of PDEs using Chebyshev spectral methods, *J. Comput. Phys.*, **228** (2009), 1480–1503. https://doi.org/10.1016/j.jcp.2008.10.043
29. S. Oh, An efficient spectral method to solve multi-dimensional linear partial different equations using Chebyshev polynomials, *Mathematics*, **7** (2019), 90. https://doi.org/10.3390/math7010090

AIMS Press